Available online at www.garmian.edu.krd

Passer Journal of Basic and Applied Sciences

Passer 8 (Issue 1) (2026) 221-227

Original Article

Preparation of CdS and Se/SeO_2 by Laser Ablation for Photodetector Applications

Zahraa Majed Hassan[1], Wedian Kadhoum Abad[2], Ahmed Naji Abd[*1]

[1]*Department of physics, College of Science, University of Mustansiriyah, Baghdad, Iraq.*
[2]*Department of Applied Science, University of Technology, Baghdad, Iraq.*

Received 09 September 2025; revised 1 December 2025;
accepted 28 December 2025; available online 05 January 2026

DOI: 10.24271/PSR.2025.546146.2351

ABSTRACT

This work describes the successful synthesis of Cadmium sulfide and selenium nanoparticles using pulsed laser ablation in liquid (DW). The analysis of the morphological structural, optical, and chemical properties of all samples has been conducted. From XRD, it found the Se, SeO2 and Se2O5 phases with average Crystalline size 10.84 nm and 19.37 nm, respectively. By FE-SEM of CdS and Selenium/Selenium Oxide was used to study the morphologies of the films, where The particles diameters was 90.89 nm. and 50.51 nm respectively. Using atomic force microscopy (AFM)of CdS and selenium/selenium oxide films were found to have average grain sizes of 40.14 and 32.07 nm, respectively. CdS nanoparticles have a band gap of 2.5 eV, while selenium/selenium oxide was discovered to have a band gap of 4.49 eV. The vibrational and functional groups found in the CdS and Selenium/Selenium oxide system have been studied by recording the FTIR spectra of CdS and Selenium/Selenium oxide NPs at room temperature. This work also describes the design of three common CdS/Si (D1), Se-Selenium oxide/Si (D2), and Se-Selenium oxide/CdS/Si(D3) Heterojunction photodetectors. The D1 detector's response spectrum shows good selectivity for VIS and NIR light detection. For optoelectronic applications, CdS NPs could therefore be a promising candidate material. It was discovered that case D2 exclusively responds to NIR light. In contrast, D3 has a reaction to both visible and infrared light.

Keywords: Selenium , Porous silicon, Heterojunction, Photodetector.

1 Introduction

Because of their distinct optoelectronic, biological, and quantum confinement effects, semiconductor nanoparticles (NPs) in colloidal fluids have drawn the attention of numerous researchers [1–3].When the particle's radius is similar to the exciton's Bohr radius compared to the bulk material, the effects of low dimensionality have a significant impact on the physiochemical characteristics of semiconductors. The easy production of II-VI semiconductor nanoparticles in the desired size range generally draws more attention. With a direct band gap (Eg) of 2.42 eV, (CdS) is one of the most promising semi-conductors among them due to its use in a number of applications, such as photo-detectors, photo-catalysts, and antibacterial properties. CdS nanoparticles were produced using a variety of methods, such as a sol–gel template, the Solvo-thermal pathway, hydrothermal, laser ablation, and chemical process [4–7]. A member of the chalcogen family, selenium is a p-type semi-conductor with a variety of condensed state forms, including amorphous, trigonal, rhombohedral, monoclinic, cubic, and orthorhombic polymorphs. With an energy band gap of about 1.7 eV, this material may convert sunlight into electricity, a process known as photovoltaic action. Researchers have recently been motivated to transform selenium into a variety of significant nanomaterial's, including ZnSe, CdSe, and others, due to its remarkable reactivity towards a wide range of chemicals. Both pure selenium and nanomaterials incorporating selenium have superior photoelectrical, semiconductor, and biolo-gical activity capacities [8,9]. Compared to previous approaches, (PLAL) is the most current technique for creating nanoparticles and has attracted a lot of interest as a cutting-edge NP manufacturing method [8]. The PLAL process is a physical synthesis method for NPs that removes the need for a chemical reaction. Because no harmful or dangerous gasses are released, it is environmentally beneficial. The ultrapurity of the resulting colloidal solutions and nanoparticles makes it easier to employ them in in vivo biological or biochemical applications. This procedure creates nanoparticles as a colloidal suspension, which increases safety when compared to dry-processed nanoparticles. Numerous variables, such as laser wavelength, laser energy, number of laser pulses, type of colloid solution, and

* Corresponding author
E-mail address ahmed_naji_abd@yahoo.com (Instructor).
Peer-reviewed under the responsibility of the University of Garmian.

pulse time, might influence the characteristics of produced nanoparticles employing this technique [10,11]. In this study, we report the synthesis of CdS and Se nanoparticles by ablation of CdS and Se targets in distilled water using a Nd:YAG laser. We investigate CdS/p-Si, Se(/p-Si), and Se(SexOx-1)/CdS/p-Si's structural, optical, and photodetecting characteristics. Cadmium sulfide (CdS) finds widespread use in various applications, particularly photodetectors. However, its efficiency is impacted by the high recombination rate and the sluggish electron–hole pair separation rate. The selenium or selenium oxide has unique optical and electrical characteristics, such as good electron conductivity and a high absorption coefficient in the red range. However, we review of previous studies has not found any publications that discuss the integration of CdS with Se or selenium oxide, especially when it comes to using this combination to create photodetectors that can operate throughout a broad wavelength range. Enhancing the separation of electron-hole pairs and decreasing recombination boosts conversion efficiency and improves the material's chemical stability. The goal of this work was to close this gap by combining the two materials in order to boost the photoresponse efficiency and improve the optical and electrical characteristics. Therefore, we indicate that this is the first report of a cadmium disulfide/selenium oxide photodetector.

2 Preparation of samples

The cadmium sulfide (CdS) and selenium (Se)99.9% pure powders used to prepare the targets were sourced from the university's laboratory. According to the data, the average particle size of these powders is approximately 4 µm, which is within the common range for non-nano powders. Using 3 g of CdS and Se in a pressing mold using a hydraulic press under a pressure of 10 tons for 30 min to form cohesive, homogeneous target suitable with diameter 1.7 cm for laser ablation as seen in Fig.1(a,b) CdS and Se respectively. The CdS and Se nanoparticle suspension was created by pulsed laser ablation(Nd:YAG laser beam- (type HUAFEI)) utilizing laser energy 480 mJ at wavelength of 1064 nm, 7ns pulse width ,a laser frequency of 5 Hz 1000 pulse where the ablation time 200sec. Following initial testing to strike a balance between ablation efficiency and particle quality, the laser energy 480 mJ and frequency (5 Hz) were chosen as shown in fig1(c). As a result, 480 mJ and 5Hz was determined to be the ideal amount, producing stable nanoparticles with a limited size range and an appropriate ablation rate. During the ablation process, Some of the laser energy is lost as it passes through the water, but in our experiment the water level above the target was as low as 2 mm, so the loss is very small (less than 5%) and practically negligible, and therefore does not significantly affect the results. The CdS and Se targets were placed separately in the bottom of a glass vessel with 5 ml of distilled water (DW).The targets and the laser lens were about 12 cm apart with spot size 2.3mm. The optimal conditions for the synthesis of CdS and Se nanoparticles(as seen in fig.1(d) with stable optical characteristics that are appropriate for photodetector applications were met using these criteria . Following preparation the solutions (CdS and Se) were put in quartz cells to investigate UV-Vis and FTIR analysis. To investigate the XRD, FE-SEM and AFM the solution was deposited by drop cast onto a glass substrate about 4 drop (with size 50 µl) to form thickness about 200∓10 nm according preliminary experiments.

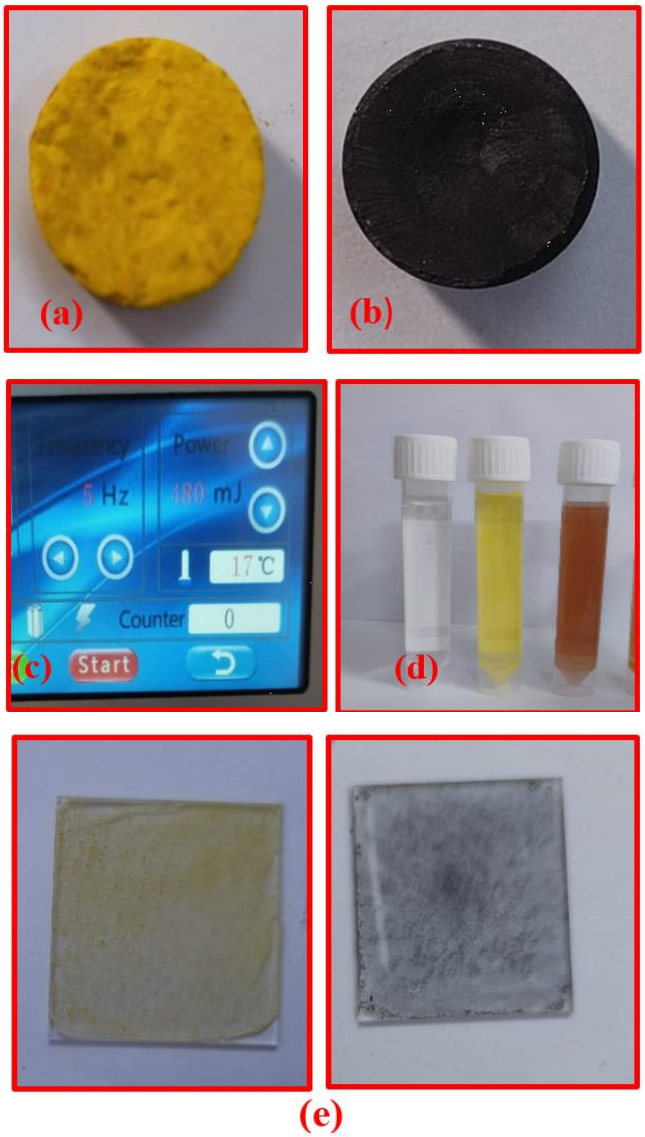

Figure 1: Experimental steps of preparation : (a,b) Target of CdS and Se respectively. (c) parameter of laser device and (d,e) suspension and thin film CdS and Se respectively.

The substrates of Silicon were cut into 2cm *2cm To get rid of the oxide, the substrates p-Si (111) with an electrical resistance of 3–5 Ω•cm) were treated with an HF:H2O (1:10) solution .Then rinsed with deionized water. The second step was to place the silver paste as electrode on the back side of substrate, then dried at 50C.The third step was thin films deposited by drop casting CdS and Se-Se2O5) NPs on the surface Si (4 drops with size 50mL) at less than 90C, to fabrication three common CdS/Si, Se -Se2O5/Si, and Se -Se2O5/CdS/Si Heterojunction photodetector as shown in Figure 2 (These devices are called devices D1, D2, and D3).

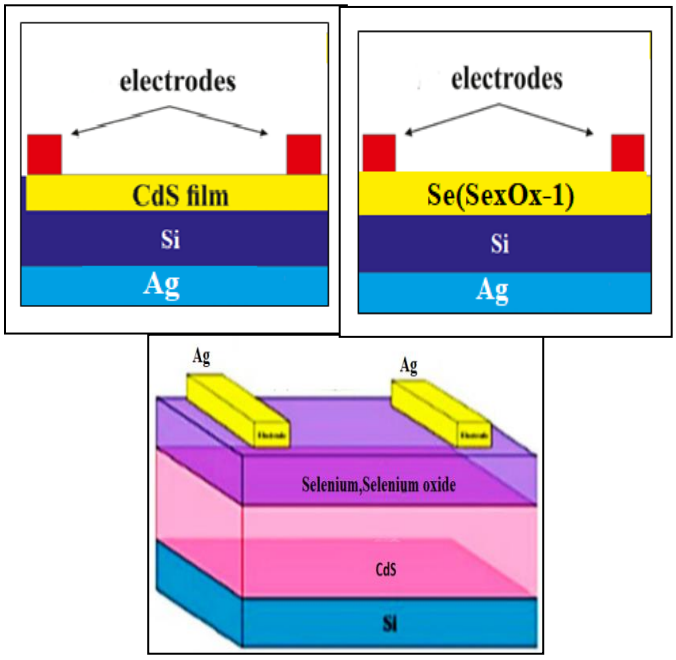

Figure 2: Schematic diagram of three Heterojunction Photodetector.

3 Results and discussion

Figure 3a,b shows the CdS and Se X-ray diffraction pattern. According to numerous research studies and in accordance with the information in the ICDC (No.00-041-1049) file card, "the diffraction peaks at 2θ correspond to the following lattice planes: (100), (002), (101), (110), and (103), respectively. Film has hexagonal wurtzite phase of CdS. The peak sharp at (100) and absence of any peaks associated with contaminants indicate to CdS sample good crystallinity and a high purity [12,13]. The Se nanoparticles' X-ray diffraction pattern is displayed in Figure 3b. The diffraction peaks at 23.55°, 29.75°, 41.90°, 43.90°, and 56.35° are indexed as the (100), (101), (110), (102), (111), (201), (112) Se planes, respectively. this agree with standard card "JCPDS card No. 06-0362" and can be indexed as the hexagonal structure of Se. The (320), (401), and (422) planes at peaks 38.9, 46.00, and 61.70, respectively, and they are in good agreement with those on the standard card (JCPDS card No. 22-1314) of SeO2. The phase of Se2O5 detected at 50.75 and 78.6 is indexed for (126) and (333) planes of Se2O5. These are in good agreement with those on the standard card (JCPDS card No. 34-1000). [14]. According to Scherer's equation, the crystallite sizes of selenium and CdS were 19.37 nm and 10.84 nm, respectively.

The morphologies of the films were examined using FE-SEM of CdS and Selenium/selenium oxide with varying magnifications of 1 µm and 200 nm. Figure 4a displays the surface of the cadmium sulfide film, where two distinct particle shapes were observed: rods covered with aggregation of semi-spherical nanoparticles (as indicated by yellow circles and lines) with a diameter of up to 90.89 nm. Figure 4b displays the Se/Selenium oxide FE-SEM images. Thin films of Se/Selenium oxide, as seen in Fig.4b, have a sponge-like structure and are porous, suggesting a sizable surface area. The particle diameter reaches 50.51 nanometers, in addition to the small clusters of nanoparticles dispersed across the sponge surface.

To investigate the surface characteristics and morphology of CdS and Selenium/Selenium oxide, atomic force microscopy (mode AA3000 Scanning Probe Angstrom Advance Inc.)) analysis was performed using a three-dimensional topographic picture with scan area (X=0.16µm and Y=0.16µm as in images) and histogram as illustrated in figures 5a-d. To provide more precise and trustworthy results, the AFM measurements were made twice at various surface regions. The program Imager 6.2 was used to analyzed the data. It was found that the nanoparticles produced using the laser ablation process and deposited by drop-cast onto substrates were extremely small, uniformly distributed, tapered, half-sphere-shaped, and occasionally monopod rod-shaped. According to the histogram, software determined that the average grain size of CdS was 40.14 nm, whereas that of Selenium/Selenium oxide was 32.07 nm. The average roughness (Sa) of CdS and Selenium (Selenium oxide) was 1.53 and 1.78 nm, respectively. Selenium/Selenium oxide was found to be more rough than CdS. This result is consistent with the idea that a decrease in mean crystal size will make a nanomaterial rougher [15].

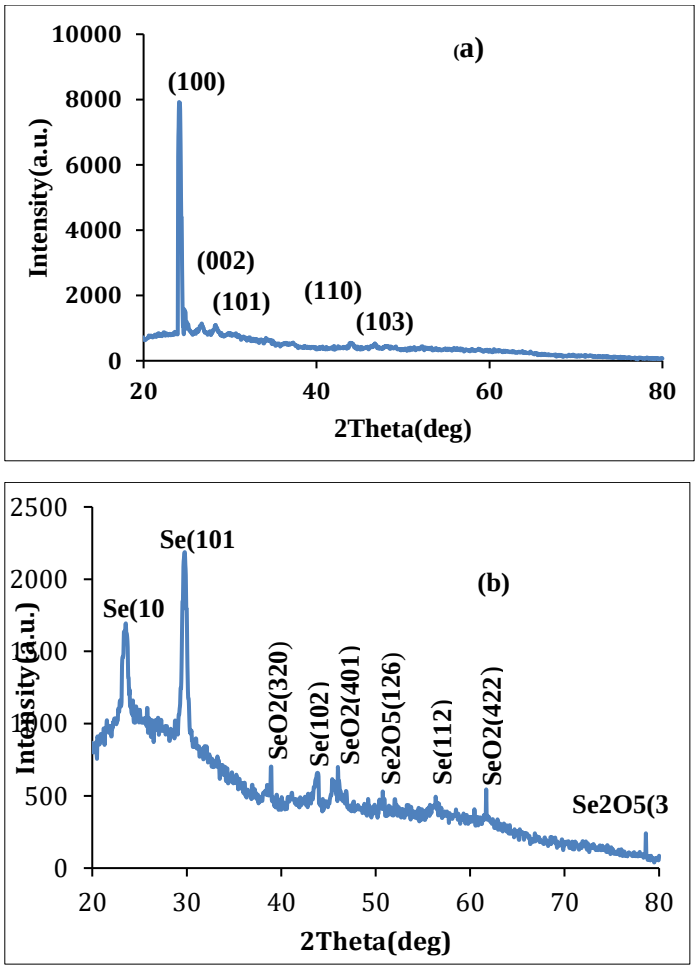

Figure 3: XRD analysis of samples of a-CdS film and b- Se film.

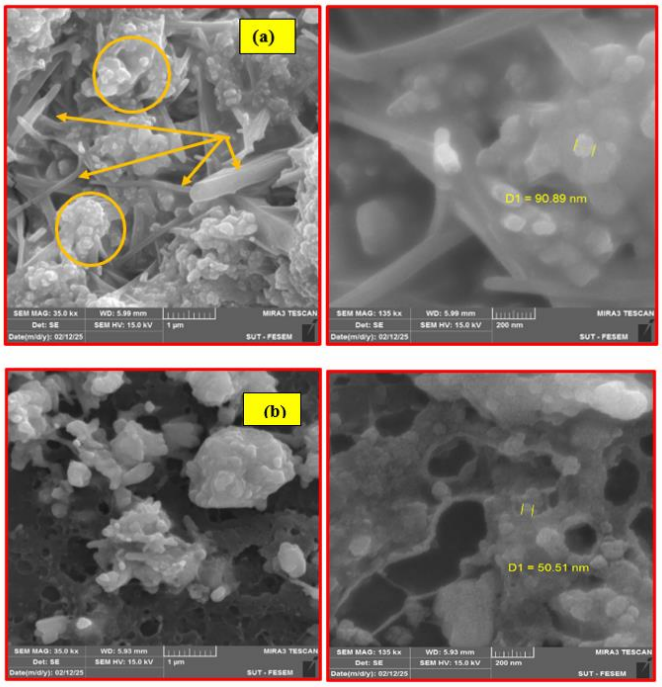

Figure 4: SEM image of samples a-CdS and b-Se/selenium oxide.

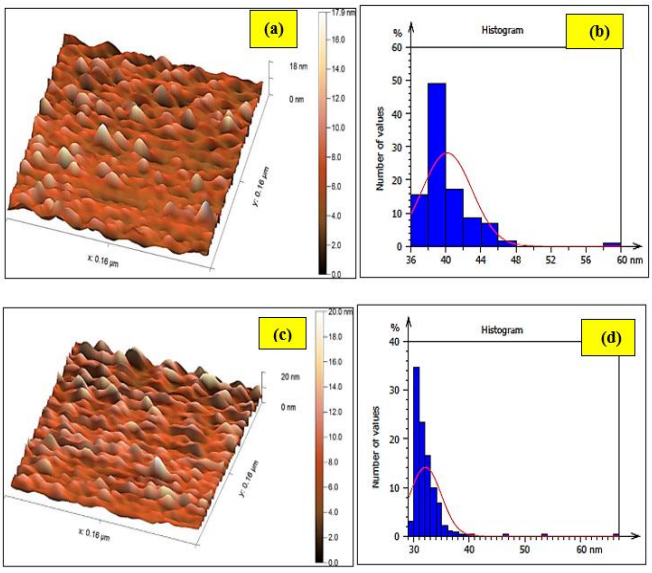

Figure 5: AFM image and Histogram of samples: (a,b)-CdS film and (c,d)-Se/selenium oxide film.

To determine the kinetic behavior of CdS NPs and Se/Selenium oxide NPs were analyzed using a PerkinElmer UV-Vis spectro-photometer, Lambda-19. The samples were scanned between 200 and 1100 nm at a speed of 480 nm/min, Figure 6a displays the CdS NPs' absorption spectra. It observed the absorbance is decrease at long wavelengths Since CdS has a high transmittance was between 91 and 96% , this indicated to can be employed as window layer in photovoltaic applications. Figure 6b The synthesis of Selenium/Selenium oxide NPs was confirmed by the wide band that was observed at the wavelength of 200-400 nm, where the absorption maximum in this region. This band appears to be attributed to the electronic transition from the valence to the conduction band in the Selenium/Selenium oxide-NPs [16]. The Tauc formula (1) was used to determine the direct optical band gap for CdS and Selenium/Selenium oxide NPs derived from the optical absorption spectra:

$$(\alpha h\upsilon)^n = A(h\upsilon - Eg) \quad (1)$$

The energy gap is denoted by E_g, the optical absorption coefficient by α, Planck's constant by h, the frequency of light by υ, the proportionality constant by A, and the direct band gap energy by n = 2[17]. The straight part of the graph $(\alpha h\upsilon)^2$ versus (hυ) was extrapolated on the energy axis at α = 0 to determine the band gap. The graphs displayed a distinct line in the linear fitting region, which was chosen to be between 2.0 and 3.0 eV for CdS and 4.0 and 5.0 eV for Se/selenium oxide. Because of the linear fitting precision, the potential experimental uncertainty in Eg estimation is ±0.05 eV. .Regarding this plot (Figure 7a,b), Figure 7a shows that the CdS nanoparticles' band gap is 2.50 eV [18]. This band gap energy CdS NPs is higher than experimental values reported by other authors 2.43, 2.46 and 2.36 eV for CdS . In comparison to the comparable absorption band edge of bulk CdS (2.42eV) , this energy gap value shows a significant blue-shift about 0.08 eV ; this shift indicates a quantum size impact in the produced CdS NPs .In figure 7b, the band gap energy of selenium/selenium oxide was determined to be 4.49 eV. Compared to previously reported band gaps 2.1 ,2.5 and 3.1eV, this band gap energy for selenium/selenium oxide nanoparticles is greater. The small nanoparticle size achieved in this work, as shown by XRD, AFM, and SEM, may be connected to these variations in band gap energy. Additionally, the quantum confinement effect will cause the band gap to widen when the particle size is lower than the Bohr excitation radius, resulting in a blue shift of the band gap energy for selenium/selenium oxide-NPs in comparison to its bulk counterpart. Therefore, according to other writers, the band gap energy decreases with increasing particle size. Thus, based on our observations, it can be said that the size of the nanoparticles significantly affects the optical absorption spectra of selenium and selenium oxide nanoparticles, leading to larger band gaps for small-sized nanoparticles [19–22].

The vibrational and functional groups found in the CdS and Selenium/Selenium oxide system have been studied by recording the FTIR spectra of CdS and Selenium/Selenium oxide NPs at room temperature (Figure 8). The strong vibrations at 3439, 1636 for CdS , and 3448, 1640 cm^{-1} for Selenium/Selenium oxide, due to the adsorbed water molecules on the surface of the CdS and Selenium/Selenium oxide, which corresponds to the O-H group. The peak at 1118 cm-1 according to reference [24] due to vibrational modes of H2O. The peaks at 2925,2853 for CdS and 29.27,2859 for Selenium/Selenium oxide have been assigned to asymmetrical and symmetrical vibrations of CH group,CH2 respectively [23,25] The C-N bond band was seen in both plots at 1386 and 1387 cm−1 [10,24]. In both graphs, the stretching of

carboxyl groups is represented by the values 1464 cm−1 and 1469 cm^{-1}. The lower wave number zone, or below 700 cm^{-1}, is where the Cd–S stretching frequency is typically observed [15]. A medium-wide absorption peak around 474–700 cm^{-1} that is associated with Cd–S stretching has been seen in our CdS nanoparticles. Selenium NPs with groups Se–O are represented by the bands at 486–823 cm^{-1} [26,27].

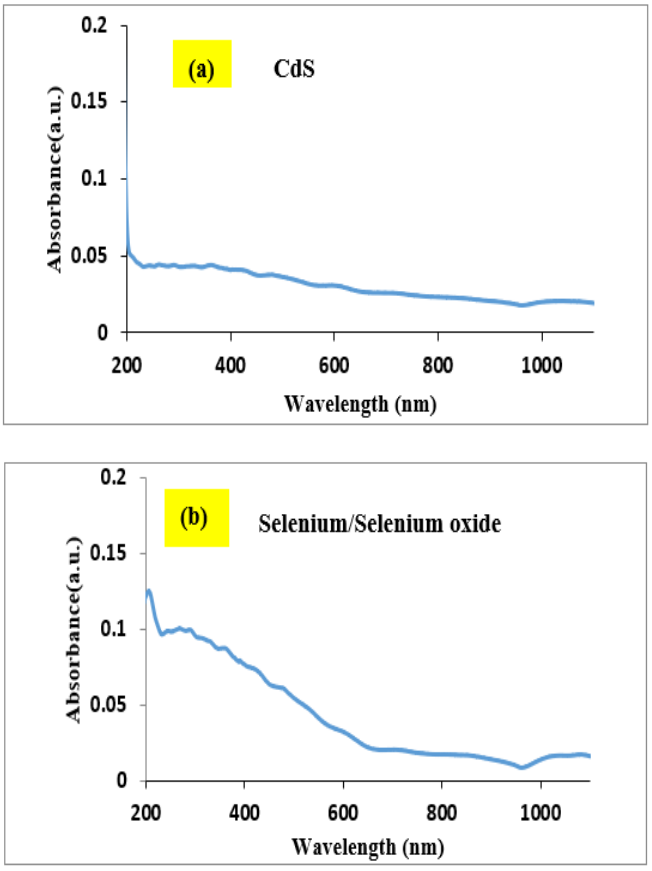

Figure 6: Absorbance spectra of a-CdS and b-Selenium/Selenium oxide NPs.

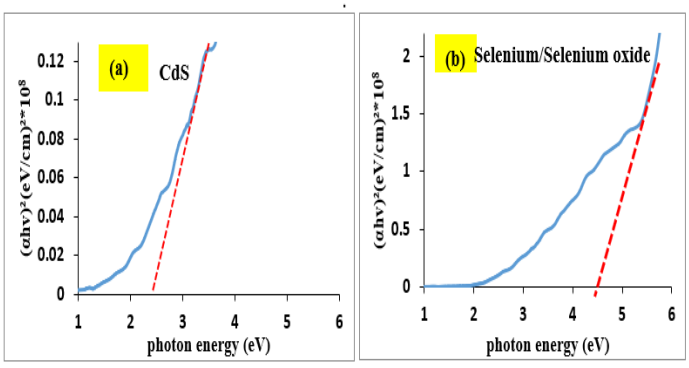

Figure 7: A graph displaying the energy band gap of a-CdS and b-Selenium/Selenium oxide.

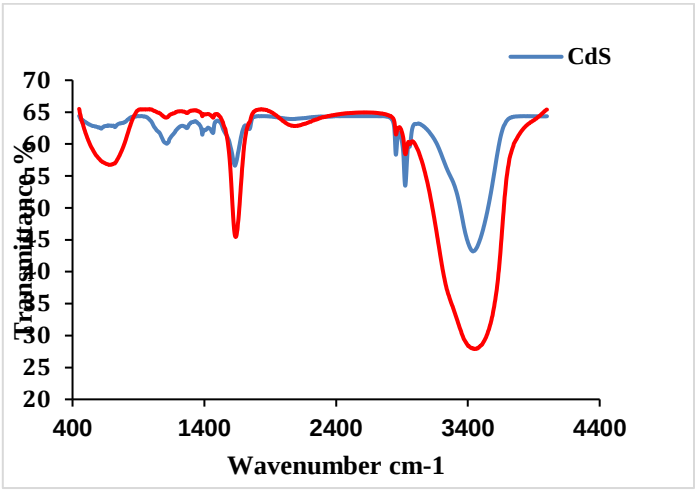

Figure 8 : FT-IR spectra of CdS and Se(SexOx-1).

The two crucial metrics used to assess photodetectors are responsiveness (R) and detectivity (D). "The ratio of photocurrent (Iph) to incident optical power (Popt)" has been calculated as a function of wavelength in order to determine the responsivity (R) [28,29]:

$$R = Iph/Pin\ (A/W) \quad (2)$$

The wavelength-dependent spectral responsivity (Rλ) for the CdS/Si (D1), Se/Si (D2), and Selenium/Selenium oxide/CdS/Si (D3) heterojunction at 5 V in the 350–1000 nm range is displayed in Figure 9a–c. The response spectrum of D1 shows that this detector has good selectivity for VIS light detection at wavelengths between 550 and 600 nm and the NIR-region between 850 and 900 nm. For D1(CdS/Si), the maximum photoresponsivity peaked at approximately 550 and 900 nm, at 0.34 A/W and 0.50 A/W, respectively. Since CdS is a window for visible light, the optoelectronic properties showed that CdS/Si had strong responsivity in the visible and near-infrared bands because of the short circuit formed by the Si substrate. The CdS energy band gap of 2.25 eV was in agreement with the cutoff at 550 nm [28–30]. Because of the absorption edge of Si, the responsivity increased at 850 after decreasing at higher wavelengths due to increased surface recombination and decreased penetrating light. The response spectra of example D2 shows that there is a single, distinct peak at 850 nm [31,32]. This shows that the photodetector only reacts to near-infrared light with a wavelength of about 850 nm. 0.89 A/W is its maximal photoresponsivity. Because of parasitic light absorption in Se(SexOx-1) through band-to-band absorption, it seldom reacts to UV and VIS light. Due to the absorbance edges of selenium, selenium oxide/CdS hetero-junction, CdS/Si heterojunction, and Si substrate, case D3 (Se/CdS/Si heterojunction) showed three peaks at 450, 600, and 850 nm. The responsivity was 0.07 A/W, 0.23 A/W, and 0.84 A/W, respectively.

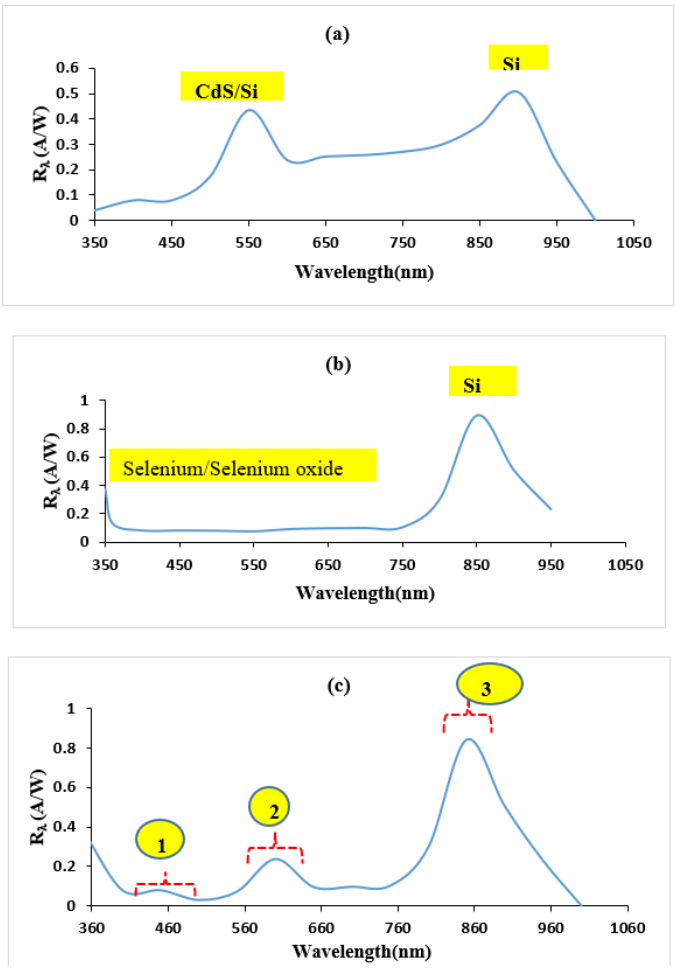

Figure 9: Responsivity of as a function of wavelength for three Photodetectors synthesized :(a) CdS/Si , (b) Se/Si , and (c) Selenium/Selenium oxide/CdS/Si .

When comparing the results CdS/Si and Selenium-selinum oxide/Si with previous studies by researchers (, R Aljarrah 2019,Raid A. Ismaila et al 2018 and Ahmed N.Abd et al.2016) and (Alharbi, S.R.N et al al.2023) [33-36] , we found that they reached the highest value for spectral response 0.08,0.28 , 0.6 and 0.54 AW^{-1}. Also while in our results we reached the highest response in range 0.84-0.89 AW^{-1}.When CdS and selenium/selenium oxide were mixed in the same system, the resulting combination's optical and electrical properties were improved by improving carrier transport, lowering losses at the layer interface, and increasing light absorption. Consequently, we were able to acquire a spectral response that was higher than what other researchers had managed to produce.

The specific detectivity D* of devices fabricated (D1,D2 and D3) was calculated from the eq.3

$$D* = \frac{R(\Delta f S)^{0.5}}{\sqrt{2qId}} \quad (3)$$

Where $I_{noise} = (\sqrt{2qId})$, R ,f ,S ,Id are responsivity , width of band, the detector sensitive area and dark current respectively.

The detectivity for the produced CdS/Si, Se(SeOx-1)/Si, and Selenium/Selenium oxide/CdS/Si photodetectors is shown as a function of wavelength in Figure 10a-c. The figure makes it evident Responsivity has a direct impact on detectivity. The highest D* measured was 1.10 × 10^{11}Jones. 1.28 × 10^{11}Jones for D1 at wavelengths of 550 nm and 900 nm respectively. The detectivity for D2 was 2.26× 10^{11} Jones at 850 nm. Lastly, the detectivity in the Selenium/Selenium Oxide/CdS/Si Photodetector was 0.19 × 10^{10} , 0.60 × 10^{10} and 2.14× 10^{11} Jones at 450, 600, and 850 nm respectively. In comparison to those common silicon-base transparent conductive oxides, the spectrum detectivity value is low. This could be because of two factors: (i) may be a strong lattice mismatch between Se(SexOx-1) with CdS and Si, which creates trap charges at recombination sites; and (ii) high resistivity, which contributes to high series resistance.

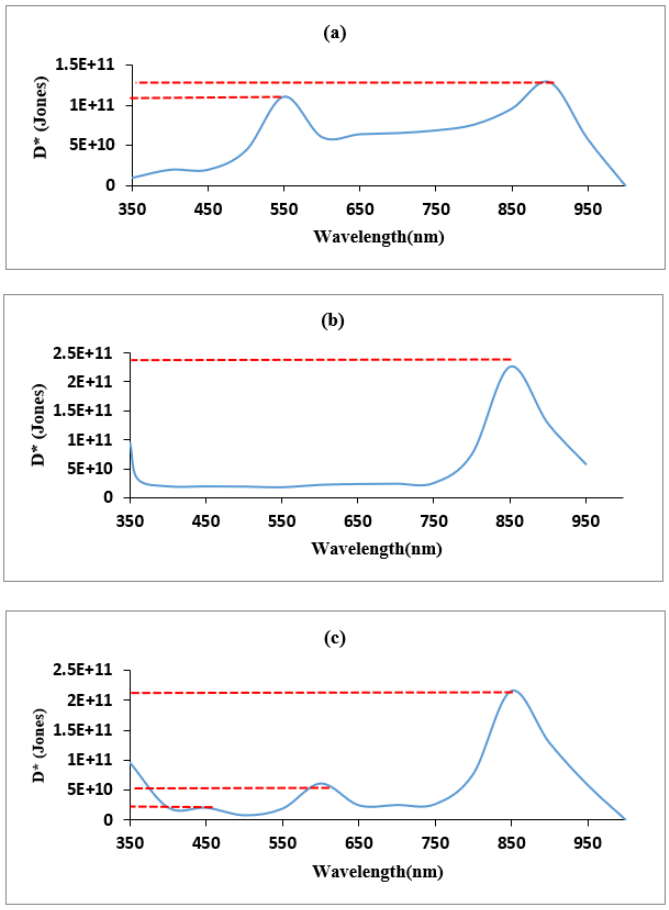

Figure 10: Detectivity for three Photodetectors synthesized: :(a) CdS/Si, (b) Se/Si , and (c) Selenium/Selenium oxide/CdS/Si.

Conclusion

We succeeded in preparing of CdS and selenium /selenium oxide nanoparticles by laser ablation and studying their properties. The results were good for making photodetectors that work in specific regions of the electromagnetic spectrum. The detectors D2 and

D3 achieved the highest detection at the wavelength between 850-900 nanometers, reaching 2.14-2.26*10^{-11}Jones. These results indicate the possibility of using the prepared materials in photodetectors, sensors, and solar cells.

Future Recommendations

Structural defects, such as material mismatches or potentially thin layers, could be the cause of the D3 Se(SexOx-1)/CdS/Si's decreased responsivity and specific.

References

[1] Zang, J., Zhao, G. & Han, G. Preparation of CdS nanoparticles by hydrothermal method in microemulsion. *Front. Chem. China* **2**(1), 98–101, doi:10.1007/s11458-007-0020-x (2007).

[2] Al-Hussam, M.A. & Jassim, S.A. Synthesis, structure, and optical properties of CdS thin-film nanoparticles prepared by chemical bath technique. *J. Assoc. Arab Univ. Basic Appl. Sci.* **11**(1), 27–31, doi:10.1016/j.jaubas.2011.10.001 (2012).

[3] Kumar, S. & Sharma, J.K. Stable phase CdS nanoparticles for optoelectronics: A study on surface morphology, structural and optical characterization. *Mater. Sci.–Pol.* **34**(2), 368–373, doi:10.1515/msp-2016-0033 (2016).

[4] Abad, W.K., Maki, S.A. & Alattar, F.I.M. Fabrication and characterization of FTO/CdS/CdTe/Al solar cell. *AIP Conf. Proc.* **2372**(1), doi:10.1063/5.0066104 (2021).

[5] Yang, F., Tian, X., Zhang, K., Zhang, X. & Liu, L. Morphology–property effect and synergetic catalytic effect of CdS as electrocatalysts for dye-sensitized solar cells. *ECS J. Solid State Sci. Technol.* **7**(6), 311–316, doi:10.1149/2.0111806jss3 (2018).

[6] Seoudi, R., Shabaka, A.A., Kamal, M., Abdelrazek, E.M. & Eisa, W. Dependence of spectroscopic and electrical properties on the size of cadmium sulfide nanoparticles. *Physica E* **45**(1), 47–55, doi:10.1016/j.physe.2012.07.006 (2012).

[7] Ismail, R.A., Khashan, K.S. & Alwan, A.M. Effect of CdS nanoparticles incorporation on porous silicon photodetectors. *Silicon* **9**(3), 321–326, doi:10.1007/s12633-016-9446-4 (2017).

[8] Van Overschelde, O., Guisbiers, G. & Snyders, R. Green synthesis of selenium nanoparticles by excimer pulsed laser ablation in water. *APL Mater.* **1**(4), (2013).

[9] Langi, B., Shah, C., Singh, K., Chaskar, A., Kumar, M. & Bajaj, P.N. Ionic liquid-induced synthesis of selenium nanoparticles. *Mater. Res. Bull.* **45**(1), 668–671, doi:10.1016/j.materresbull.2010.03.005 (2010).

[10] Zeng, H. et al. Nanomaterials via laser ablation/irradiation in liquid: A review. *Adv. Funct. Mater.* **22**(1), 1333–1353 (2012).

[11] Kareem, M.M. Effect of laser shots on morphological and optical properties of CuO nanoparticles prepared by Nd:YAG laser. *Passer J. Basic Appl. Sci.* **3(1)**, 200–206, doi:10.24271/psr.33 (2021).

[12] Lee, M., Han, S. & Jeon, Y.J. pH-controlled hydrothermal synthesis of submicrometer-sized CdS spheres. *Bull. Korean Chem. Soc.* **31**(12), 3818–3821, doi:10.5012/bkcs.2010.31.12.3818 (2010).

[13] Obasuyi, A.R. et al. Synthesis and characterization of CdS nanostructures. *Ilorin J. Sci.* **1**(1), 121–127, doi:10.1016/j.physe.2009.04.020 (2014).

[14] Kumaran, S.K. et al. Influence of dietary selenium nanowires on growth performance of broiler chicken. *Int. J. Biosci. Nanosci.* **2**(4), 78–83 (2015).

[15] Abed, Z.S., Mohammad, R.K. & Elttayef, A.K. Structural properties of Ag–CuO thin films. *Egypt. J. Chem.* **65**(4), 685–691, doi:10.31257/2018/JKP/100209 (2022).

[16] Salih, A.A., Abad, W.K., Fadaam, S.A. & Hussein, B.H. Lead oxide nanoparticles via green synthesis. *Dig. J. Nanomater. Biostruct.* **18**(4), 1225–1233, doi:10.15251/DJNB.2023.184.1225 (2023).

[17] Saleh, A.M. Improvement of optical properties of Zn-doped MnO nanocomposites. *Passer J. Basic Appl. Sci.* **5**(2), 348–355, doi:10.24271/psr.2023.407846.1349 (2023).

[18] Najm, A.S. et al. Nucleation and growth mechanism of CdS thin films synthesized by CBD. *Sci. Rep.* **12**(1), 15295, doi:10.1038/s41598-022-19340-z (2022).

[19] Rahi, S.K., Al-Wardy, R.A. & Al Ogaili, H.A.T. Fabrication of SeO_2 nanoparticles from cinnamon extract. *Baghdad Sci. J.* **22**(4), 1252–1259, doi:10.21123/bsj.2024.8208 (2024).

[20] Mellinas, C., Jiménez, A. & Garrigós, M.C. Microwave-assisted green synthesis of selenium nanoparticles. *Molecules* **24**(22), 4048, doi:10.3390/molecules24224048 (2019).

[21] Jadhav, A.A. & Khanna, P.K. Microwave irradiation of selenadiazole: formation of selenium nanoparticles. *RSC Adv.* **5**(1), 44756–44763, doi:10.1039/C5RA05701A (2015).

[22] Guleria, A., Neogy, S. & Adhikari, S. Ionic-liquid assisted synthesis of amorphous Se nanoparticles. *Mater. Lett.* **217**(1), 198–201, doi:10.1016/j.matlet.2018.01.088 (2018).

[23] Rasool, K.H., Abad, W.K. & Abd, A.N. Preparation of ZnO nanoparticles from *Juglans regia* extract. *J. Biosaf. Biosec.* **7**(1), 1–8, doi:10.1016/j.jobb.2024.10.004 (2025).

[24] Gurugubelli, T.R. et al. Ni^{2+}-doped ZnO–CdS nanocomposite. *Chem. Pap.* **76**(1), 557–566, doi:10.1007/s11696-021-01888-1 (2022).

[25] Chen, G. et al. Green biosynthesis of CdS quantum dots. *Colloids Surf. B* **117**(1), 199–205, doi:10.1016/j.colsurfb.2014.02.027 (2014).

[26] Jeevanantham, V. et al. Greener microwave-synthesized Se nanospheres. *J. Mater. Res.* **38**(7), doi:10.1557/s43578-023-00965-3 (2023).

[27] Zhu, X., Kumari, D., Huang, M. & Achal, V. Biosynthesis of CdS nanoparticles. *Mater. Des.* **98**(1), 209–214, doi:10.1016/j.matdes.2016.03.008 (2016).

[28] Ali, M.Y., Al-Azzawi, M.A., Abad, W.K. & Abd, A.N. V_2O_5 and Bi_2O_3 thin films on PSi. *Silicon* **17**(1), 625–634, doi:10.1007/s12633-024-03216-0 (2025).

[29] Al-Azzawi, M.A., Ali, M.A. & Abad, W.K. Preparation of NiO/Si and ZnO/Si photodetectors. *J. Opt.* **54**(1), 712–721, doi:10.1007/s12596-024-01718-z (2024).

[30] Hammadi, O.A. & Naji, N.E. Electrical and spectral characterization of CdS/Si heterojunction. *Opt. Quantum Electron.* **48**(1), 375, doi:10.1007/s11082-016-0647-2 (2016).

[31] Habubi, N.F., Ismail, R.A., Abd, A.N. & Hamoudi, W.K. Porous silicon photodetectors with CdSe nanoparticles. *Indian J. Pure Appl. Phys.* **53**(11), 718–724 (2015).

[32] Saeed, S.I., Ali, M.A., Abad, W.K. & Abd, A. Low-cost solar cell and photodetector applications. *Int. J. Nanosci.* **23**(21), doi:10.1142/S0219581X23500631 (2024).

[33] Alharbi, S.R.N., Qasrawi, A.F. & Algarni, S.E. Selenium oxide-based laser sensors. *Opt. Quantum Electron.* **55**(1), 677, doi:10.1007/s11082-023-05003-4 (2023).

[34] Aljarrah, A. & Aljobory, A. Designing a CdS/Si photodetector. *Iran. J. Phys. Res.* **19(3)**, doi:10.47176/ijpr.19.3.20463 (2019).

[35] Abd, A.N. Improved photoresponse of porous silicon photodetectors by CdS nanoparticles. *J. Nano Adv. Mater.* **4**(1), 33–44, doi:10.18576/jnam040105 (2016).

[36] Ismail, R.A., Al-Samarai, A.M.E. & Ali, A.Y. CdS/macroporous silicon/c-Si heterojunction photodetector. *Optik* **168**(1), 302–312, doi:10.1016/j.ijleo.2018.04.101 (2018).